Elucidating the effect of poly(ethylene terephthalate) chain structure on its enzymatic degradation behaviour

*Jean-Baptiste Lena[a], Rui A. Gonçalves[a], Sharad Kharel[a], Srinivasaraghavan Kannan[b], Chandra S Verma [c,d,e], Keerthi Mohan Pinchi[b], Sierin Lim[b], Yeng Ming Lam[a]**

*Email: ymlam@ntu.edu.sg

[a] Nanyang Technological University, School of Material Sciences & Engineering, 50 Nanyang Ave, Singapore 639798

[b] Nanyang Technological University, School of Chemistry, Chemical Engineering and Biotechnology, 70 Nanyang Drive, Singapore 637457

[c] Nanyang Technological University, School of Biological Sciences, College of Science, 60 Nanyang Drive, Singapore 637551

[d] Bioinformatics Institute, Agency for Science, Technology and Research, 30 Biopolis street, Singapore 138671

[e] Department of Biological Sciences, National University of Singapore, 16 Science Drive 4, Singapore 117558

ABSTRACT:

Poly(ethylene terephthalate) (PET) is a widely used thermoplastic polymer, but its excessive use and poor waste management pose environmental challenges. Enzymatic degradation of PET offers a potential solution that is eco-friendly and yields monomers suitable for the synthesis plastics. In 2016, Yoshida et al. discovered a PET degrading enzyme (PETase) from sediment-dwelling bacteria, *Ideonella sakaiensis*. It was found that enzymatic degradation rate of PET increases with reduced crystallinity, suggesting that this parameter may be amenable to tuning.

To investigate the interplay between substrate crystallinity and chemical structure on the efficiency of PET degradation, we synthesized PET, PET copolymers (e.g., poly(ethylene terephthalate-co-ethylene isophthalate; P(ET-co-EI)), poly(ethylene terephthalate-co-ethylene phthalate); P(ET-co-EP)), and branched PET that have been used in packaging. These polymers have good properties for injection moulding and oxygen scavenging, respectively. The polymers were synthesized from aryl

chloride and ethylene glycol. Size, composition, randomness, thermal properties, and crystallinity of all polymers were determined. The polymers were then enzymatically degraded to compare the efficiency of PETase on the different PET substrates. Our study demonstrates that while chemical modification reduces crystallinity, the influence of chemical structures (the kinks and branches) on the binding of the PETase, and hence the enzymatic degradation, is more significant than the effect of crystallinity.

Keywords: Polyethylene terephthalate, chemical modification, crystallinity, structural characterization, thermal properties, enzymatic degradation

Introduction

Over the last century, plastics have become increasingly ubiquitous and their global production exceeds 9 billion tons at present[1]. This is due to its versatility and low cost of production. Among all the plastics, polyethylene terephthalate (PET) stands out due to its good thermal and mechanical properties, thermal and chemical resistance[2, 3], low gas permeability, high impact strength[4], and good processability[5]. A semi-crystalline polymer, PET is the one of the most widely used thermoplastic in the world and in 2020, over 30 million tons were produced worldwide. It represents 18 % of the global polymer production. The main applications for PET are in packaging[6, 7] and textile industries[8]. Currently, PET is the most recyclable plastic produced. PET bottles have more than 50 % recycling efficiency within the European Union[9]. However, a significant proportion of PET falls out of the current waste management systems and ends up in our environment where it takes 450 years to degrade. About 80% of the plastic has been landfilled, 10 to 12% was incinerated and less than 10% was recycled. The uncontrolled use, combined with the lack of waste management especially in the developing countries make PET a heavy contributor to the global plastic pollution issue[10]. It is thus necessary to minimize PET wastes.

The most common method of PET waste management is mechanical recycling. PET are recycled through extrusion. Recycled PET (rPET) can be mixed with pristine PET (pPET) to yield plastics that retain most of the properties of pPET. This allows the use of the plastic in the same or similar applications prior to the recycling referred to as closed-loop recycling. Alternatively, rPET can be used for different applications that do not require as good mechanical properties as pPET (e.g., from packaging to clothes) referred to as open-loop recycling[6, 11]. Mechanical recycling allows the extension of the lifetime of PET and requires less than half the energy used to generate new plastics from petroleum resources [REF]. Nevertheless, at the end of its life-cycle, a large amount of PET still ends up in environment. Alternative recycling methods should be developed. Chemical depolymerization, such as methanolysis or glycolysis, transforms PET into monomers or oligomers that can be re-used to produce PET. This method, called tertiary recycling, has promising results as it allows operating in a closed loop in mild conditions. However, it sometimes requires high temperature and pressure as well as the use of toxic chemicals[12]. Biodegradable PETs can be synthesized by copolymerizing PET and degradable aliphatic polyesters such as poly(lactic acid) (PLA). This however requires a long time (more than 10 weeks) for their complete degradation[13]. Furthermore, their application is limited as they may shatter and form microplastics[10].

Another possibility is the enzymatic degradation of PET. Enzyme-based depolymerization is more sustainable than chemical depolymerization as it requires milder pH, lower temperature and no toxic reagents. Moreover, enzymes have high selectivity, targeting the polymer ester bonds which allows recovery of the monomers[12]. The first important PET depolymerization was reported in 2005 by Müller et al. A cutinase from the thermophilic bacterium *Thermobifida fusca* could degrade 50 % of PET bottle film at 55 °C within 3 weeks[14]. Since then, numerous enzymes capable of degrading PET have been reported[12]. In 2016, Yoshida et al. identified an efficient PET-degrading enzyme, PETase, from the bacterium *Ideonella sakaiensis*. The bacterium was isolated from the soil in a plastic bottle recycling facility in Japan. This aromatic polyesterase converts PET into TPA, mono(2-hydroxyethyl) terephthalic acid (MHET) and bis(2-hydroxyethyl) terephthalic acid (BHET)[15]. Many studies have demonstrated

that enzymatic degradation occurs preferentially on amorphous parts rather than crystalline regions with poor chain mobility, and it occurs as a surface erosion process[16]. Understanding the structure of PETase, accessibility of amorphous polymer chain, and tailoring the enzymes to fit the PET substrate have become research priorities. In 2018, Austin et al. studied the structure of PETase using X-ray and demonstrated the potential of this enzyme to degrade not only PET but also other aromatic and semi-aromatic polyesters[17]. Unfortunately, it was not efficient for aliphatic polyesters. PETase have similar characteristics to lipases and cutinases[18] but with an open active site cleft that can accommodate bulky ester linkages. The aromatic rings of PET chains are at an ideal π-stacking distance to aromatic rings of the enzyme resulting in an ideal orientation and holding of ester linkage for hydrolysis. They also showed that enzymatic degradation occurs mostly on amorphous sites due to the less ordered structure as well as polymer chain mobility, and managed to optimize the enzyme with bioengineering techniques[17]. In 2020, Tournier et al. developed an LCC-based enzyme that can depolymerize 90 % of PET within 10 hours and showed that biologically recycled PET exhibit the same properties as petrochemical PET. These results suggest that enzymatic degradation is a promising method for PET waste management[19]. In 2021, Cui et al. computationally designed enhanced PETase that has greater thermal stability and that can also degrade polybutylene terephthalate (PBT) and polyethylene naphthalate (PEN). In 2022, Thomsen et al. studied the effect of PET crystallinity and glass transition temperature on the enzymatic degradation kinetics. They observed that (i) enzymatic degradation is slower for high crystallinity PET, (ii) the more crystalline the PET, the more heterogeneous is the surface modification after enzymatic degradation, and (iii) physical changes of substrates above the Tg lead to less efficient degradation[20]. In the same year, Erikson et al. compared the activity of wild-type PETase and a double mutant. They showed that the reaction temperature and the crystallinity of the substrate strongly influence their catalytic activity, and the presence of degradation products inhibits further degradation[21].

PET is produced by polycondensation from terephthalic acid (TPA) and ethylene glycol (EG) in the presence of a catalyst. First, PET oligomers are obtained, and water is eliminated by distillation.

Second, oligomers condensate and long chains PET are formed. This requires high temperature (250-300 ^{o}C) and low pressure (<1 mbar)[22]. Alternative methods have been developed to obtain PET with common equipment available in most modern chemical laboratories (e.g., from dimethyl terephthalate (DMT) and EG with a catalyst[13], or from terephthaloyl chloride (TPCl) and EG in basic media[23]). These synthetic routes result in shorter PET chains.

In recent years, PET with modified structures has attracted interest. Inserting ethylene isophthalic units in PET allows the creation of amorphous segments and due to the presence of long branches in PET, the material is more robust[24]. Copolymerization is important in tuning and balancing material properties. Several studies on the effect of branching and kinking in PET on thermal properties and crystallization are reported in the literature. Poly(ethylene terephthalate-co-ethylene isophthalate) and branched polyethylene terephthalate are used in numerous applications (e.g., PET bottles, food and packaging)[25-27]. Adding ethylene isophthalic or ethylene phthalate units allows more control over thermal crystallization during preform injection or stretch-blow modeling, and lower the melting point[28, 29]. For PET bottle, film and packaging, about 2 % of ethylene isophthalate units is added to slow down the crystallization. Branching increases the rheological properties of PET[30, 31]. Introducing branched structure is often used through chain extension during extrusion process to avoid PET losing some of the mechanical properties. In 1999, Jaykannan et al. studied the effect of linear, kinking, and branching imperfection on the crystallization process of PET. They observed that PET, as well as PET-based copolymers with linear and kink modification, promote a tri-dimensional crystal growth while branched PET exhibits a rodlike and a platelike crystal growth (one and two dimensions). They also noted that at a very low concentration of co-monomer, the nucleation is facilitated, which leads to a slight increase in crystallinity[32]. In 2019, Chen et al. synthesized long chain branched PETs and made biaxially stretching films. They demonstrated that (i) crosslinked structures were formed even if the degree of branching (*DB*, defined as the number of branches per monomer units) was lower than 3 %, (ii) a bi-dimensional crystal growth is observed for cold crystallization while both bi-dimensional and tri-dimensional crystal growth were observed for melt crystallization, (iii) crystal size increases and

crystal growth rate decreases with increasing the degree of branching, (iv) the more the PET is branched, the more it resists to hydrolytic degradation[33]. In 2010, Ubach et al. synthesized a series of copolymers containing both ethylene terephthalate and ethylene isophthalate units. They obtained random copolymers with high molecular weight and decrease of crystallinity was observed with increasing the number of ethylene isophthalate units, thereby yielding an amorphous polymer at 25 %. The crystallization rate decreases with the amount of ethylene isophthalate units. They observed Avrami coefficients between 2 and 3, indicating both bi- and tri-dimensional crystal growth. The Avrami coefficient increases with the crystallization temperature[34]. This confirmed the previous results from Li et al. and Yu et al.[35, 36]. In 2022, Avarzman et al. studied the effect of combining the addition of trimesoyl chloride (TMA) and isophthalic acid (IPA) on crystallization and randomness of modified PET. They observed that (i) insertion of both ethylene isophthalate units and branching reduced the crystallinity, (ii) the presence of isophthalate units had more effect on the crystallinity than the branching, (iii) addition of both TMA and IPA resulted in polymers with lower $\underline{T_g}$, (iv) the addition of TMA increased the randomness of polymers and (v) the particles size increased with TMA[37].

While most attributes of PET degradation (mechanism, enzyme modeling, the effect of crystallinity, degradation of other aromatic polyesters with PETase, the effect of degradation on plastic surface, physical and mechanical properties) have been studied, and some bioengineering methods to improve PETases have been developed[15, 17, 19-21, 38-42], the effect of branching and kinking in PET on enzymatic degradation remains unexplored. This may hold a crucial insight and may help us understand if PET can be chemically modified to improve enzymatic degradation, or if such chemical modification would affect the interactions between enzyme and substrate and inhibit the degradation. The implications of substrate physical properties (polymer length, crystallinity, glass transition temperature, surface area and surface charge) on PETase engineering has been previously proposed[43].

In this study, we aim to understand how the presence of branching, ethylene isophthalate units, and ethylene phthalate units affect the enzymatic degradation of PET with aromatic polyesterase derived

from *I. sakaiensis*. Linear PET, branched PETs (DB= 1 to 3 %) and copolymers of ethylene terephthalate/ethylene isophthalate (P(ET-co-EI)) and ethylene terephthalate/ethylene phthalate (P(ET-co-EP)) with different compositions were synthesized via acid chloride route. Their structures (chain length, composition, DB, randomness) were determined using ^{1}H and ^{13}C NMR spectroscopy. Thermal properties and crystallinity, as well as crystallization kinetic parameters, were determined by differential scanning calorimetry and X-ray diffraction. Finally, some of the polymers were enzymatically degraded. The quantity of degradation products (TPA, MHET, and BHET) was measured by high-performance liquid chromatography (HPLC)[44].

Experimental Section

Materials

Acetonitrile (HPLC/Spectro) and chloroform (amylene stabilized) (HPLC/Spectro) were obtained from Tedia. Terephthaloyl chloride (TPCL) ≥99%, isophthaloyl chloride (IPCl) ≥99%, phthaloyl chloride (PCl) 90 %, 1,3,5-benzenetricarbonyl trichloride (or trimesoyl chloride, TMCl) 98%, triethylamine ≥99%, ethylene glycol anhydrous 99.8%, 1,1,1,3,3,3-hexafluoro-2-propanol (HFIP) ≥99%, formic acid (reagent grade) ≥95 %, 1,2-dichlorobenzene 99% and dimethyl sulfoxide (DMSO) ≥99 % were purchased from Sigma-Aldrich. Methanol (analytical reagent grade) 99.9 % and dichloromethane 99.8 % were obtained from Fisher Scientific. Sodium hydroxide pallets (analytical reagent grade) was purchased from Schedelco, sodium dodecyl sulfate (SDS) from Hoefer Inc., and glycine from Bio-Rad. TPA, MHET and BHET are from Merck KGaA. Chloroform-D (D, 99.8 %) + 0.05 % v/v TMS + silver foil and trifluoroacetic acid-D (D, 99.5 %) were provided by Cambridge Isotope Laboratory Inc. Water was Milli-Q quality.

Polymerization

PET and PET copolymers were prepared in two steps from aryl chloride and ethylene glycol. In the first step, polymers with OH terminal on both sides are synthesized and during the second step, an

excess of polymer with OH end groups react with aryl chloride to obtain polymers with higher molecular weights. The detailed procedure of the linear PET is detailed bellow.

First step: Into a 500 mL bineck round bottom flask equipped with a condenser and a magnetic stirrer, 10 g of TPCl, (1 eq.), 3.67 g of EG (1.2 eq.) and 200 mL of dichloromethane were added. The mixture was stirred at a temperature of 0-10^{o}C in an ice bath. The flask was purged with nitrogen gas for 5 min. Then, 10 g of Et_3N (2 eq.) in 20 mL of dichloromethane were slowly added. The mixture was left in ice bath for 1 h and then at room temperature for 24 h. Then, the solvent was removed with a rotary evaporator. The polymer was washed in water, filtered under vacuum and dried overnight in vacuum oven. To remove the impurities, the dry sample was dissolved in a mixture HFIP/chloroform and filtered through cotton. Then, the polymer was precipitated in methanol (about 1 L), filtered under vacuum and dried in vacuum oven. Monomer conversion was not measured but molar mass was estimated by NMR spectroscopy.

Second step: Into a bineck round bottom flask equipped with a condenser and a magnetic stirrer, 3 g of polymer synthesized in the first step (1.2 eq.) and 25 mL of 1,2-dichlorobenzene were added. The setup was purged with nitrogen gas for 5 min. Then, the mixture was heated up to 100 ^{o}C and cooled down to dissolve the polymer. Only partial dissolution was observed. Then, 1 eq. of TPCl, 2 eq. of Et_3N (slowly poured) and 4 mL of dichloromethane were added. The exact amount of Et_3N and TPCl depends on the molar mass of the pre polymer obtained at the step 1. The mixture was left under stirring at room temperature for 24 h. Then, the solvent was removed with a rotary evaporator. The polymer was washed with water, filtered under vacuum and dried overnight in vacuum oven. Then, the sample was purified as previously described.

PET copolymers were synthesized with the same method but instead of adding 1 eq. of TPCl, experiments were carried out with 0.9, 0.8, 0.7, 0.5 eq. of TPCl and 0.1, 0.2, 0.3, 0.5 eq. of IPCL fpr P(ET-co-EI)s, as well as 0.9, 0.8, 0.7, 0.5 eq. of TPCl and 0.1, 0,2 0.3, 0.5 eq. of PCl for P(ET-co-EP)s.

Branched PET polymers were synthesized in a single step as the molar mass of the polymers were higher. The polymerization and purification were similar to the first step described previously but with 1-X eq. of TPCl, X eq. of TMCl, (1.2(1-X)+1.8X) eq. of Et_3N and 220 mL of dichloromethane. Experiments were carried out for X=0.01, X=0.02, and X=0.03.

More details are in Supplementary Information (Schemes S1 to S3 and table S1)

NMR spectroscopy

Spectra of PETs and copolymers were acquired in $CDCl_3/CF_3COOD$ (8/1 v/v) at 21 °C on an Agilent 400 MR with Bruker SamplerXpress, equipped with a OneNMR probe and variable temperature capabilities, operating at Larmor frequencies of 400.13 MHz for ^1H and 100.62 MHz for ^{13}C. The polymer concentrations for ^{13}C NMR analyses were 50 mg dissolved in 0.9 mL $CDCl_3/CF_3COOD$. For the ^1H NMR analyses, 10 mg of polymer was dissolved in a 0.9 mL of $CDCl_3/CF_3COOD$. One-dimensional ^1H NMR spectra were acquired with 36,864 data points, 256 scans, 20.485 ppm spectral width (8196.7 Hz), 1 s relaxation delay, 2.249 s acquisition time and a 25° flip angle. One-dimensional ^{13}C NMR spectra were recorded with 32,768 data points, 512 scans, 198.8 ppm spectral width (20,000 Hz), 30.0 s relaxation delay, 0.8192 s acquisition time and a 90° flip angle with inverse-gated decoupling. The chemical shift scales were calibrated for 1H and 13C NMR spectra by TMS at 0 ppm. The ^1H and ^{13}C NMR signal assignments are provided in Tables S3 and S4, and all the NMR spectra are shown in Figs S1 to SS4 and S6 to S20. One-dimensional T1-relaxation time experiments have determined that a relaxation delay of 30.0 s with an acquisition time of 0.8912 s is sufficient to ensure quantitative results (acquisition time þ relaxation delay > 5 T1) (see Fig. S5). The inversion recovery experiment was carried out with one value of t between the two pulses. Others inversion recovery experiments established that a 14.5 s and 17.5 s relaxation delay with a 0.8912 s acquisition time was insufficient for a full recovery of these signals. The inversion recovery experiments are described in detail in the Supplementary Information and in[45]. Molecular weight, copolymer composition, degree of branching (*DB*), and randomness was measured (equations S2 to S17 in Supporting information).

Differential scanning calorimetry

Polymers were analysed with a Discovery DSC (TA Instruments). Samples were accurately weighed into aluminium crucibles and crimped shut with a pierced lid. A similar empty crucible with a crimped pierced lid was used as reference. The samples were cycled in a heat-cold-heat-cold sequence from 25 to 300 °C at a rate of 10 °C min^{-1} under a high purity nitrogen gas flow of 50 mL min^{-1}. Data analyses for determining glass transition temperature T_g, cold crystallization temperature T_{cc}, melting temperature T_m, and associated enthalpies of thermal transitions during the first heating were carried out using Trios software (TA Instruments). Thermograms are presented in supplementary date (Figure S22).

Percent crystallinity X_c was calculated as follows[19]:

$$X_c(\%) = \frac{\left(\Delta H_f - \Delta H_{cc}\right)}{\Delta H_{f100}} \quad (1)$$

where, ΔH_f is the enthalpy of fusion associated with the melting transformation (endothermic) and ΔH_{cc} is the enthalpy associated with the cold crystallization transformation (exothermic), both events during the first heating cycle. ΔH_{f100} represents the enthalpy of fusion of PET polymer with 100% crystallinity. The value used was retrieved from literature as 140.1 J g^{-1} [46, 47]. All the thermal analyses were conducted on as-synthesized polymer samples. The results are reported as the average of three measurements and associated standard deviation.

Wide-angle X-ray scattering

The X-ray measurements were conducted using the simultaneous small- and wide-angle X-ray scattering instrument Nano-inXider (Xenocs), equipped with a micro-focus source generating X-rays of a wavelength λ = 1.542 Å (Genix3D), operating at 50 kV and 0.6 mA. Each polymer sample was exposed to X-ray radiation for 600 s in medium resolution mode (flux of 600 Mph.s^{-1}; beam size on sample of 800 µm). The collected 2D images were integrated into 1D background-subtracted profiles

using XSACT software (Xenocs). Silver behenate standard was used to calibrate the instrument. The degree of crystallinity was determined by subtracting the scattering of the molten polymer sample (amorphous) from the as-synthesized sample. The scattering profiles are presented in figure S23. Data are in table S5.

PETase production

PETase production was carried out using *E. coli* Shuffle cells (NEB) containing pET-22b plasmid encoding the PETase gene from *I. sakaiensis* . LB medium (1L) was inoculated with 2% overnight culture, supplemented with 100 µg/ml ampicillin. The culture was incubated at 30 °C with constant shaking (180 rpm) until OD_{600} reached 0.5 followed by 0.5 mM isopropyl β-D-1-thiogalactopyranoside (IPTG) induction. The culture was then incubated at 16 °C for 20 hours. Cells were harvested and pellets were stored at -80 °C until further use. Cell pellets were suspended in 70 ml lysis buffer (50 mM Tris-Cl, 500 mM NaCl, pH 7.4). Cells were lysed using sonication (37% amplitude, 20 minutes, 5 sec pulse ON and 5 sec pulse OFF). Supernatant was collected after spinning in ultracentrifuge (145,000x*g*, 30 mins). Imidazole (20 mM) was added to the supernatant and PETase was purified in a HisTrap column using AKTA GO FPLC system (Cytiva). Fractions containing PETase were pooled together, and protein concentration was measured using Bradford assay (Bio-Rad Laboratories, Inc.). Protein was desalted and concentrated in 100 mM phosphate buffer (pH 8) and brought to a concentration of 8 mg/ml using 10 kDa Amicon MWCO filters. Equal volume of 100% glycerol was added, and the enzyme was stored at -20 °C until further use. All reactions would use this enzyme stock.

Enzymatic degradation

Polymer sample (2 mg) was suspended in 500 µL reaction media comprising of 200 µL DI water, 230 µL glycine-NaOH buffer (50 mM, pH 9.0) and 70 µL of PETase stock (20 mM) for degradation analysis. As a negative control, PETase was substituted with equal volume of additional DI water. 28 Eppendorf tubes (duplicates with and without enzymes for 7 polymers) of reaction mixtures were placed in a

thermos-shaker (Biofrontier) operated at 30 °C with a speed of 1500 rpm for 24 h and 72 h for the first and second series of experiments, respectively. After these time points, the Eppendorf tubes were centrifuged at 21,100x*g* for 5 mins and the supernatant was collected for HPLC analyses.

HPLC analyses

The samples were analysed using 1260 Infinity HPLC (Agilent Technology) connected to a UV/Vis detector (G1314A WD) and C18 column (Eclipse Plus C18, 5 µm, 4.6 x 150 mm) was used. Mobile phase A was water containing 1% formic acid and mobile phase B was acetonitrile and the flow rate was fixed at 1 $mL.min^{-1}$. The mobile phase was changed gradually from 5 % to 25 % mobile phase A over 15 min, remained at 25 % mobile phase A for 2 min, 25 % to 5 % mobile phase A for 1 min, and remained at 5 % mobile phase A for 5 min. The detection wavelength was set at 260 nm. All experiments were performed in duplicate. Samples consisted of 200 µL of supernatant, 200 µL of water, and 200 µL of DMSO. In these conditions, TPA is expected to appear at 10 min, MHET at 12.5 min and BHET at 14 min. The relationship between peak area to TPA, MHET, and BHET concentration was obtained with calibration curves (Figures S24 to S26). HPLC chromatograms are presented in Supporting information (Figures S27 to S34).

SEM analyses

The sample powder was dispersed in water (5×10^{-1} mg mL^{-1}). The dispersion was drop-casted on aluminium, air dried, and was subsequently coated with an ultrathin Pt layer to minimize charging. The SEM images were obtained using a Schottky field emission scanning electron microscope (JEOL JSM-7800FPRIME), at an acceleration voltage of 5 kV. Magnifications of 100, 500, 5000, and 10000 were used. Images are in Supporting information (Figure S35).

Docking

The crystal structure of double mutant (R103G/S131A) *I. sakaiensis* PETase in complex with ligand HEMT (PDB ID 5XFZ; resolution 1.5 Å) was used to model the binding of PETase with linear PET and with modified PET molecules. The crystal structure was modified to construct the PETase structure by

modelling the two residues (G103 and A131) back to the wild type sequence (G103R and A131S). The 3D structures of the linear and modified PET molecules were built using the *Maestro* module and minimized using the *Macromodel* module employing the OPLS-2005 force field[48] in the program Schrödinger 12.0[49]. All the PET molecules were then prepared with *Ligprep* module in Schrödinger that generates low energy tautomers and enumerates realistic protonation states at physiological pH. The prepared molecules were docked into the binding pockets on the surface of PETase using the *Glide*[50]module of Schrödinger. A box of size 10 x 10 x 10 Å for molecular docking centred on the selected active site residues (S131, H208, D177) was used to confine the search space of each docked PET molecule. For the grid generation, the default *Glide* settings were used. Docking was carried out using standard protocols[51] and the docked conformation of each PET molecule was evaluated using the *Glide* Extra Precision (XP) scoring function.

The predicted complexes of PETase with the PET molecules were further refined using Molecular Dynamics (MD) simulations. MD simulations were carried out with the *pmemd.cuda* module of the program Amber18[52]. The partial charges and force field parameters for each PET molecule were generated using the *Antechamber* module in Amber. All atom versions of the Amber14SB force field (ff14SB)[53] and the general Amber force field (GAFF)[54] were used to model the protein and the PET molecules respectively. The *Xleap* module of Amber was used to prepare the systems for the MD simulations. All the simulation systems were neutralized with appropriate numbers of counter ions.

Each neutralized system was solvated in an octahedral box with TIP3P[55] water molecules, leaving at least 10 Å between the solute atoms and the borders of the box. All MD simulations were carried out in explicit solvent at 300 K. During the simulations, the long-range electrostatic interactions were treated with the particle mesh Ewald[56] method using a real space cut off distance of 9 Å. The Settle[57] algorithm was used to constrain bond vibrations involving hydrogen atoms, which allowed a time step of 2 fs during the simulations. Solvent molecules and counter ions were initially relaxed using energy minimization with restraints on the nonhydrogen atoms of the enzyme-PET complex structures. This

was followed by unrestrained energy minimization to remove any steric clashes. Subsequently the system was gradually heated from 0 to 300 K using MD simulations with positional restraints (force constant: 50 kcal mol^{-1} $Å^{-2}$) on the nonhydrogen atoms of the enzyme-PET complex structures over a period of 0.25 ns allowing water molecules and ions to move freely. During an additional 0.25 ns, the positional restraints were gradually reduced followed by a 2 ns unrestrained MD simulation to equilibrate all the atoms. Finally, production MD simulations were carried out on each system for 100 ns in triplicates. Simulation trajectories were visualized using VMD[58] and figures were generated using PyMOL[59].

Results and discussions

Microstructure of PETs and copolymers

The size, degree of branching (*DB*) and copolymer composition of the synthesized copolymers were determined by NMR spectroscopy. The results are shown in Table 1. Pre polymers obtained after the first step were also characterized. Results are in Table S2. For all P(ET-co-EI), copolymers compositions are equal to batch compositions. This agrees well with previous literature results[22, 34, 35]. However, results are surprising for P(ET-co-EP) and branched PETs. For these polymers, we noticed that the fraction of ethylene phthalate units in copolymers are always lower than the fraction of PCl in the batch. For branched PETs, *DB* values are lower than expected. TMCl fractions of 0.01, 0.02 and 0.03 leads to PETs with less than 1, 2 and 3 % of branching respectively. The reason will be explained in detail later.

For the P(ET-co-EP), it was observed that the Mn of these copolymers are mostly lower than the Mn of P(ET-co-EI). This suggested that some of the PCl did not react to form the copolymers. For the polycondensation of two monomers, Carothers equation can be written as follows:

$$\overline{DP_n} = \frac{1 + r}{1 + r - 2rp} \qquad (2)$$

where p is the overall conversion and r represents stochiometric ratio of the reactants. If a monomer is in excess, $r < 1$ and so DP_n becomes lower for each value of p. A possible reason is the occurrence of side reactions that would lead to the formation of cyclic compounds, favoured by the geometry of ortho aromatic rings. Refer to Scheme 1. Another possibility is a slower rate of reaction when IPCl is replaced by PCl, leading to lower conversion and thus smaller chains.

Table 1. Size, *DB* and copolymer compositions of the synthesized polymers

Polymers	**Batch composition**	**Copolymer composition**	***DB* (%)**	DP_n	M_n **(g.mol^{-1})**
Linear PET	TPCl: 1 eq, EG: 1.2 eq.	-	-	33.3	6,400
Branched PET 1	TPCl: 0.99 eq., TMCl: 0.01 eq., Prepol: 1.2 eq.	-	0.75	37.5	7,200
Branched PET 2	TPCl: 0.98 eq., TMCl: 0.02 eq., EG: 1.2 eq.	-	1.53	31.5	6,000
Branched PET 3	TPCl: 0.97 eq., TMCl: 0.03 eq., EG: 1.2 eq.	-	2.06	46.3	8,900
P(ET9-co-EI1)	TPCl: 0.9 eq., IPCl: 0.1 eq., Prepol: 1.2 eq.	F_{ET}=0.90, F_{EI}=0.10	-	141.1	27,100
P(ET8-co-EI2)	TPCl: 0.8 eq., IPCl: 0.2 eq., Prepol: 1.2 eq.	F_{ET}=0.79, F_{EI}=0.21	-	53.1	10,200
P(ET7-co-EI3)	TPCl: 0.7 eq., IPCl: 0.3 eq., Prepol: 1.2 eq.	F_{ET}=0.73, F_{EI}=0.27	-	58.9	11,300
P(ET1-co-EI1)	TPCl: 0.5 eq., IPCl: 0.5 eq., Prepol: 1.2 eq.	F_{ET}=o.47, F_{EI}=0.53	-	87.0	16,700
P(ET95-co-EP5)	TPCl: 0.9 eq., PCl: 0.1 eq., Prepol: 1.2 eq.	F_{ET}=0.95, F_{EP}=0.05	-	36.5	7,000
P(ET9-co-EP1)	TPCl: 0.8 eq., PCl: 0.2 eq., Prepol: 1.2 eq.	F_{ET}=0.90, F_{EP}=0.10	-	70.8	13,600
P(ET8-co-EP2)	TPCl: 0.7 eq., PCl: 0.3 eq., Prepol: 1.2 eq.	F_{ET}=0.81, F_{EP}=0.19	-	29.2	5,600
P(ET7-co-EP3)	TPCl: 0.5 eq., PCl: 0.5 eq., Prepol: 1.2 eq.	F_{ET}=0.70, F_{EP}=0.30	-	32.3	6,200

Prepol: pre polymer obtined after the first step

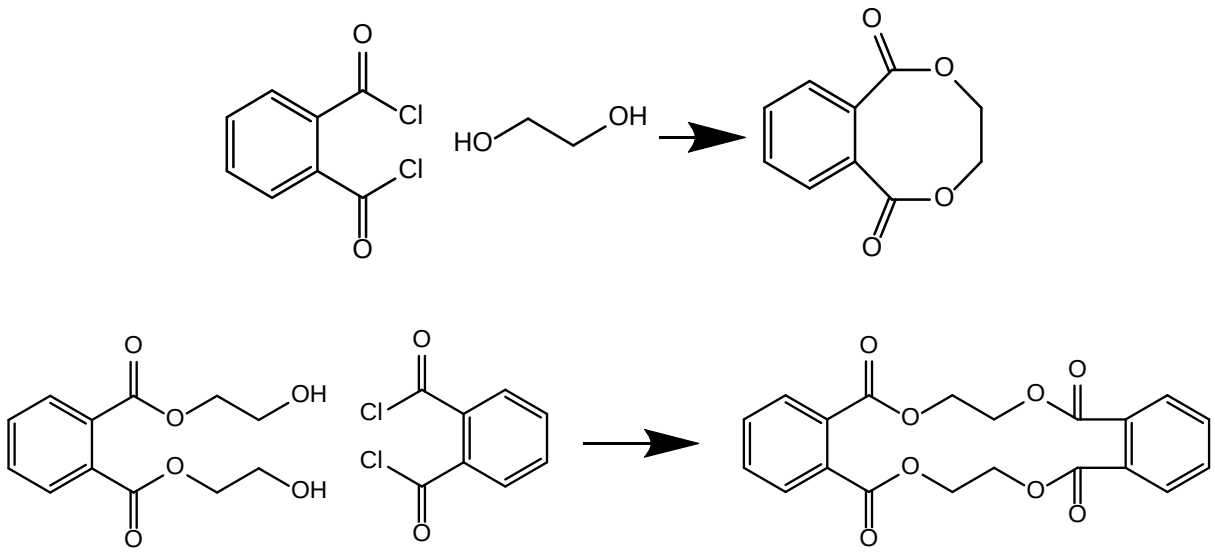

Scheme 1. Potential side reactions that can occur during the polymerization of EG, TPCl and PCl.

For the branched PETs, even though the size of branched PET is lower than the size of P(ET-co-EI), the hypothesis that side reactions involving TMCl is highly unlikely as (i) the amount of TMCl is very low, so side reactions would have limiting effects on the stoichiometry, and (ii) branched PETs were synthesized in one step while copolymers were made in two steps. We note that for these branched PETs, the Mn is significantly higher than what would be predicted by Carothers equation. This is due to the presence of aromatics rings with three connecting point which make this equation not applicable. It is known that the presence of branching and crosslinked structure reduces the solubility of polymers. Dissolution of polymers is a complex process that is often underestimated. It was demonstrated previously that for starch and poly(acrylic acid), transparent liquids were shown by NMR spectroscopy to still be incompletely dissolved solids[60-62]. Accuracy of *DB* measurement can be lowered by incomplete dissolution of PETs. The solubility of PETs in $CDCl_3$/TFA-D was tested by comparing ^{1}H NMR spectra of linear and branched PETs using the normalized peak area to noise ratio. The "peak area to noise ratio" (PNR) is defined as the absolute peak area divided by the noise. The peak area is the quantity proportional to the amount of sample and the noise is used as a scaling factor to put all spectra on the same scale. The normalized *PNR* is defined as follows:

$$Normalized\ PNR = \frac{PNR}{[Sample] \times \sqrt{number\ of\ scans}} \quad (3)$$

In this instance, signals of hydrogen linked to aromatic carbons of ethylene terephthalate units were used to measure the normalized *PNR*. Results are presented in Figure 1.

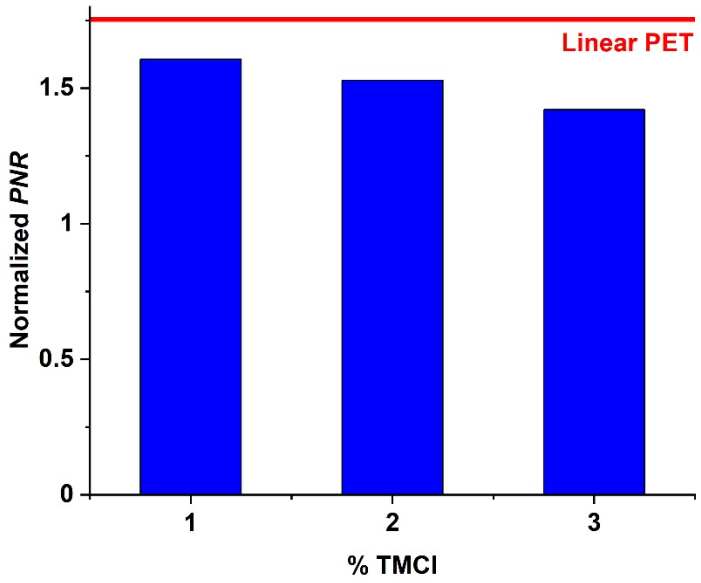

Figure 1. Normalized PNR of linear PET (obtained after the first step of polymerization), branched PET 1, branched PET 2 and branched PET 3 related to the amount of TMCl.

From Figure 1, we can observe that the normalized PNR is reduced by the number of branches. Consequently, *DB* may be underestimated due to the presence of insoluble fractions whose branching is not detected. This reduction in solubility may indicate that in cases where lower values of *DB* compared to fractions of TMCl are found, crosslinked structures may already be formed.

^{13}C NMR spectra were used to determine the microstructure of P(ET-co-EI) and P(ET-co-EP) chains. Sequence distributions of P(ET-co-EI) and P(ET-co-EP) can be determined using signals of the aromatic quaternary carbons of ethylene terephthalate units (triads) and ethylene isophthalate/ethylene phthalate units (dyads) (Figure 2). Average sequence lengths η and randomness R of copolymers could be calculated with Eq. S12 to S17. Results are shown in Table 2.

(a)

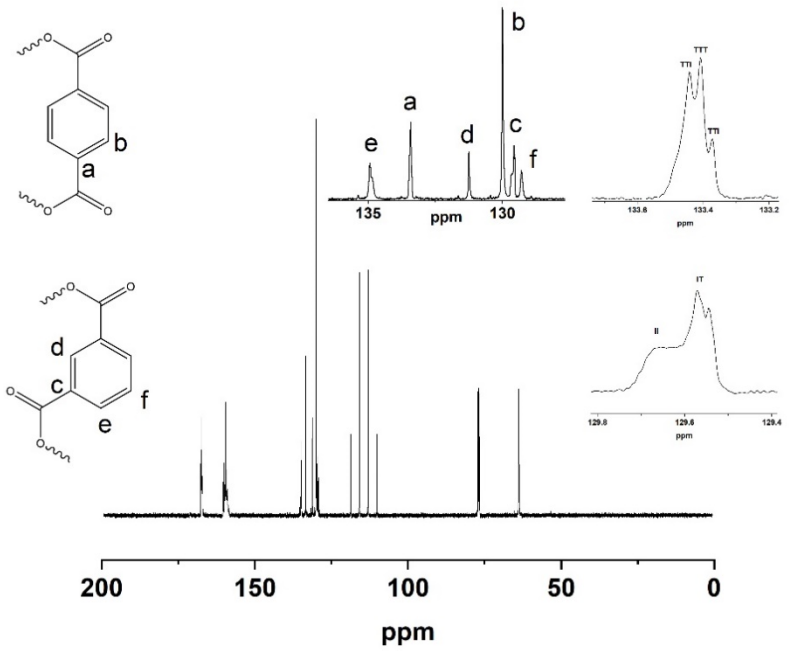

(b)

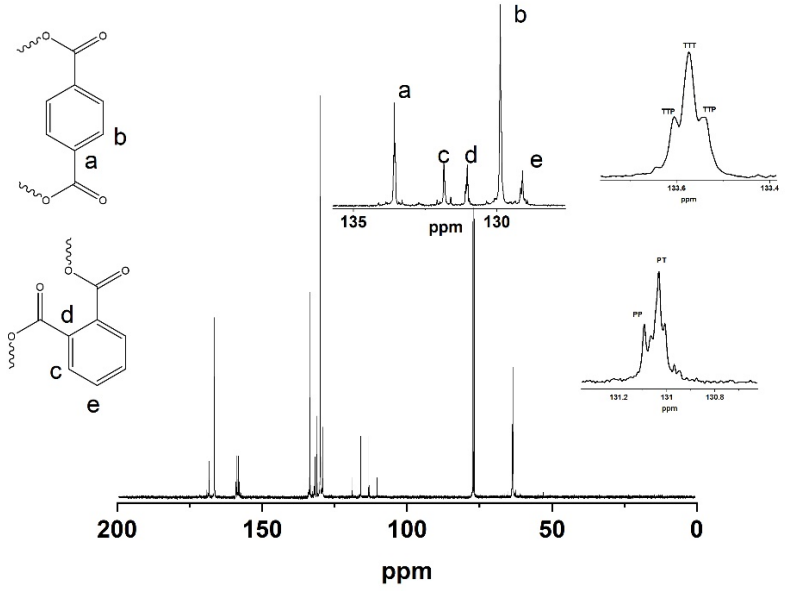

Figure 2. ^{13}C NMR spectra with signal attribution of aromatic carbons as well as sequence distributions for (a) P(ET8-co-EI2) and (b) P(ET8-co-EP2).

Table 2. Average sequence length and randomness of copolymers

Polymer	η_T	η_I	η_P	Randomness
P(ET9-co-EI1)	NM	NM	-	NM
P(ET8-co-EI2)	4.32	1.56	-	0.87
P(ET7-co-EI3)	3.27	1.47	-	0.99
P(ET1-co-EI1)	1.69	2.13	-	1.06
P(ET95-co-EP5)	15.29	-	1.24	0.87
P(ET9-co-EP1)	10.82	-	1.36	0.84
P(ET8-co-EP2)	7.04	-	1.55	0.79
P(ET7-co-EP3)	4.62	-	2.10	0.69

NM=not measured. Triads were not visible on the ^{13}C NMR spectrum. η_T, η_I and η_P are the average sequence lengths of ethylene terephthalate, ethylene isophthalate and ethylene phthalate units respectively.

The randomness or degree of randomness corresponds to the fraction of segment of a copolymer in which monomers residues are distributed randomly. The closer the randomness value is to unity, the more each monomers are located randomly in the copolymer molecule. Lower randomness values mean more blocky structures. P(ET-co-EI)s are mostly random, which confirmed previous literature results[34, 37]. As for P(ET-co-EP)s, the results are different. The insertion of ethylene phthalate units seems to favour blocky structure. Several hypotheses can be raised. First, Ubach *et al*. observed that high conversions favours random copolymers[34]. As explained previously, phthaloyl chloride may lead to lower final conversions. Second, we observe much higher ethylene terephthalate average sequence length in P(ET-co-EP) than in P(ET-co-EI). This is consistent with more blocky structures.

Thermal properties and crystallinity

Thermal analysis of all the synthesized PET powders was conducted to determine key thermodynamic properties such as glass transition temperature (T_g), cold crystallization temperature (T_{cc}), fusion temperature (T_f), and associated enthalpies. These allowed us to calculate the percentage of crystallinity, using the method described in materials and methods, and those values are presented in Table 3.

Table 3. Differential scanning calorimetry parameters of PET polymers. T_g – Glass transition temperature, T_{cc} – cold crystallization temperature, ΔH_{cc} – enthalpy of cold crystallization, T_f – fusion temperature, ΔH_f – enthalpy of fusion.

Polymer	T_g (°C)	T_{cc} (°C)	ΔH_{cc} (J g^{-1})	T_f (°C)	ΔH_f (J g^{-1})	Crystallinity (%)
Linear PET	72.7 ± 3.1	99.2 ± 5.5	15.5 ± 0.8	252.2 ± 3.1	62.2 ± 1.7	33.3 ± 0.8
P(ET9-co-EI1)	76.0 ± 0.2	107.9 ± 0.4	17.3 ± 0.8	227.1 ± 0.7	38.4 ± 0.5	15.1 ± 0.3
P(ET8-co-EI2)	77.7 ± 1.6	122.1 ± 0.0	19.9 ± 0.4	208.9 ± 1.0	26.9 ± 0.4	5.0 ± 0.2
P(ET7-co-EI3)	69.8 ± 0.1	-	-	182.2 ± 2.2	-	-
P(ET1-co-EI1)	70.3 ± 5.0	-	-	-	-	-
P(ET95-co-EP5)	76.5 ± 1.0	107.9 ± 0.4	8.1 ± 0.4	232.6 ± 0.2	52.3 ± 0.4	31.5 ± 0.5
P(ET9-co-EP1)	64.7 ± 0.2	103.8 ± 0.4	9.8 ± 0.3	222.1 ± 0.8	46.0 ± 0.2	25.8 ± 0.2
P(ET8-co-EP2)	62.0 ± 0.8	124.8 ± 0.2	3.3 ± 0.3	199.2 ± 0.6	39.6 ± 1.7	25.9 ± 1.2
P(ET7-co-EP3)	50.9 ± 3.1	-	-	-	-	-
Branched PET 1	56.4 ± 0.0	98.9 ± 1.1	7.3 ± 0.1	235.4 ± 0.6	55.5 ± 0.6	34.4 ± 0.5
Branched PET 2	63.6 ± 3.9	-	-	235.2 ± 2.0	50.4 ± 0.9	35.9 ± 0.6
Branched PET 3	72.3 ± 0.2	106.4 ± 0.3	12.0 ± 0.9	237.8 ± 3.2	55.0 ± 0.4	30.7 ± 0.4

Linear PET is expected to have sufficient free volume to allow for chain segment mobility at relatively lower temperatures, and indeed, its T_{cc} was found to be 99.2 °C, with an enthalpy of 15.5 J g^{-1}. The linear PET exhibited 33.3% crystallinity. The maximum degree of crystallinity that can be achieved by isothermal cooling (C_{max}) can be calculated from the enthalpy of melting divided by the enthalpy of melting of PET polymer with 100% crystallinity. In this case, C_{max} was found to be 44.4%, indicating that the degree of solid-state crystallization was 11.1%.

The replacement of ethylene terephthalate (ET) units with ethylene isophthalate (EI) led to a progressive disappearance of the cold crystallization, fusion, and melting crystallization peaks (Figure S22), confirming that the incorporation of EI units breaks the ordered sequences and reduces the crystalline properties of the polymer chains, as previously reported[22, 34, 35]. A slight increase in T_g for P(ET-co-EI-1) and P(ET-co-EI2) was detected, which could be a result of the increased in the number averaged molecular weight (M_n). This increase in M_n led to a decrease in chain end concentration, hence a decrease in free volume at the end group region. Furthermore, when the ratio of ET equaled EI, only one thermal transformation was detected (Figure S22e), indicating that the polymer was amorphous[35]. However, our results did not show a clear correlation between DP_n and T_g. This lack of trend might be due to the compensation between both the effect of EP incorporation and the effect of chain length. Previous studies have shown different results; for example, Ubach et al. demonstrated

a clear decrease in T_g with the incorporation of EI units[34], whereas Jayakannan et al. found that linear and kinked polyesters exhibit similar T_g values[63]. The fusion temperature (T_f), which represents the temperature at which entire chain movement occurs, was found to decrease with EI substitution, likely due to lower intermolecular bonding resulting from the reduced crystallinity. Notably, the presence of 10% EI led to a reduction in crystallinity of about 55%, or ca. 85% with double the amount of EI units compared to linear PET.

The replacement of ET units with ethylene phthalate (EP) units resulted in a less significant decrease in crystallinity compared to the replacement with ethylene isophthalate (EI) units, which could be attributed to the differences in microstructure and average sequence length discussed in section 3.1. The P(ET-co-EP) copolymers have more blocky microstructures and longer ethylene terephthalate average sequence lengths, resulting in less disruption of ET segments and less disorder created. Additionally, the incorporation of EP units led to a reduction in M_n, but this did not show a clear trend due to differences in monomer conversion. However, we observed that P(ET-co-EP) chains were overall shorter than P(ET-co-EI) chains and branched chains, which may exhibit higher crystallinity. The T_g was found to be lower with the incorporation of EP units, consistent with other studies in literature[34]. More amorphous chains mean more flexibility, resulting in a lower T_g. Similarly, an increased amount of EP led to a more complex thermal behaviour, as observed for the polymers with larger quantities of EI.

The incorporation of branched groups resulted in a less significant effect on the crystallinity of the polymers, while it was more effective in reducing the T_g and T_f.=. Branching can affect polymer motion in two ways, which in turn can affect the T_g. Firstly, local chain motion is reduced due to smaller average linear chain length, resulting in a higher T_g. Secondly, branching increases the number of chain ends, which improves segmental mobility and leads to lower T_g. In this work, we observed a decrease in T_g from 0 to 1% branching, followed by an increase from 1% to 3% branching. The resulting effect showed little trend, which confirms previous literature findings that no influence of branching on T_g

was observed[64-67]. Moreover, we would not expect significant variation of T_g with such a low *DB*. The effect of reducing local motion may become dominant over increased segmental mobility above 1% branching. Formation of a chemical crosslinked network at higher branching degrees led to fewer end groups and hence a higher T_g. It is important to note that the PETs synthesized in this work have OH terminal groups, which are capable of forming hydrogen bonds, leading to an increased T_g. The number of branches influences the density and proximity of OH groups, which also affects the T_g. In 2012, Khalyavina *et al*. similarly reported no clear influence of branching degree on T_g for aromatic-aliphatic polyesters with OH end groups[68].

Wide-angle X-ray scattering (WAXS) was utilized in this study to assess the degree of crystallinity of seven PET powder samples[69], including linear PET, P(ET9-co-EI1), P(ET8-co-EI2), P(ET9-co-EP1), P(ET8-co-EP2), branched PET (*DB*=2%), and branched PET (*DB*=3%). The WAXS results were then compared to the crystallinity measurements obtained from differential scanning calorimetry (DSC). This enabled the correlation between WAXS and DSC data to be established and the effects of the various monomer units and degrees of branching on the crystallinity of the PET samples to be determined.

Figure 3a shows the scattering profiles of the synthesized PET powders after being exposed to X-ray radiation for 600 s (as described in Materials and Methods). The powders do not show anisotropy, as evidenced by the absence of oriented intensity profiles. After subtracting the scattering profile of the molten polymer (amorphous) from the profile of the as-synthesized polymer, the degree of crystallinity can be determined based on the X-ray peak intensity (Figure S26 and Table S6). A comparison plot with both the degree of crystallinity determined using DSC and that determined using WAXS is presented in Figure 3b. Despite the distinct methodologies employed by each technique to assess crystallinity, the trend observed is consistent. The WAXS data exhibits a decrease in crystallinity with the incorporation of EI units and a less notable reduction with the incorporation of EP or polymer branching, which has been previously explained.

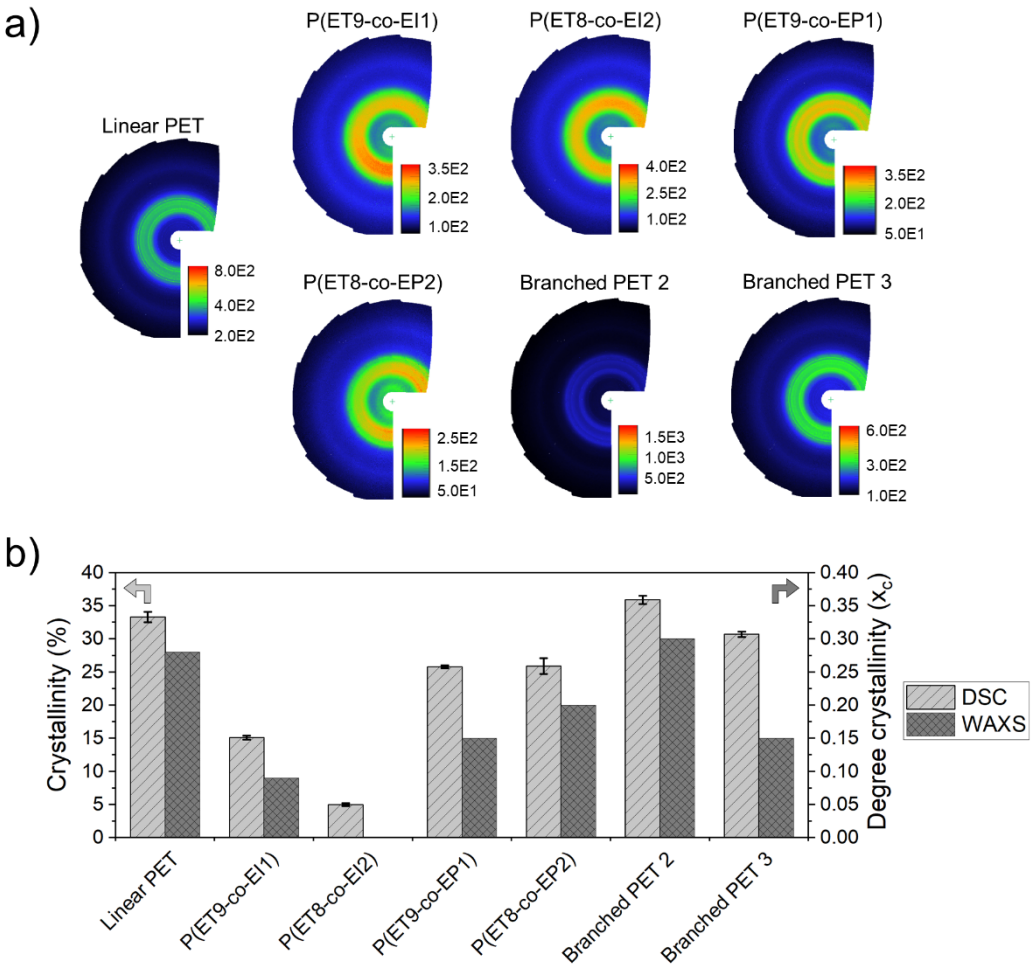

Figure 3. Crystallinity determination of PET polymers. a) 2D wide-angle scattering profiles and b) crystallinity (%, determined using DSC) and degree of crystallinity (%, determined using WAXS) of linear PET, P(ET9-co-EI1), P(ET8-co-EI2), P(ET9-co-EP1), P(ET8-co-EP2), branched PET (*DB*=2%), and branched PET (*DB*=3%).

Enzymatic degradation of PETs and PET-based copolymers

To examine the effect of substrates on the enzymatic degradation, linear PET, branched PET 2, branched PET 3, P(ET9-co-EI1), P(ET8-co-EI2). P(ET9-co-EP1), and P(ET8-co-EP2) were incubated with PETase in glycine buffer at pH 9 for 24 h and 72 h. The percentage of degraded PET was calculated based on the amounts of TPA and MHET detected by HPLC and quantified with the calibration curves.

Details are given below, and the results are presented in Table 4. Likewise, the amount of PET degraded in correlation to the crystallinity of the PET is shown in Figure 4.

In the degradation medium, PET was degraded at a concentration of 4 g.L^{-1}. Experiments for 24 h and 72 h degradation were set up separately. To calculate the amount of PET degraded, we assumed that 1g of PET degraded will lead to 1 g of degradation product (Eq. 4).

$$PET\ degraded\ (\%) = \frac{([TPA] + [MHET])}{4} \times 100 \qquad (4)$$

The product concentrations are expressed in g.L^{-1}.

Table 4. Percentage of degraded PET measured by HPLC of supernatant of degradation medium for each polymer after (a) 24 h and (b) 48 h of incubation at 30 °C temperature.

Polymers	% degradation after 24h of incubation	% degradation after 72h of incubation
Linear PET	27.9±0.4	28.1±1.0
P(ET9-co-EI1)	25.4±0.2	25.8±0.0
P((ET8-co-EI2)	22.7±0.8	20.9±0.6
P(ET9-co-EP1)	25.8±0.1	25.5±0.1
P(EY8-co-EP2)	1.8±0.1	2.2±0.9
Branched PET 2	13.8±0.3	11.5±0.2
Branched PET 3	17.4±4.8	28.7±0.6

Both experiments (incubation for 24 h and incubation for 72h) were carried out separately. *SD* was calculated with Excel based on each duplicate.

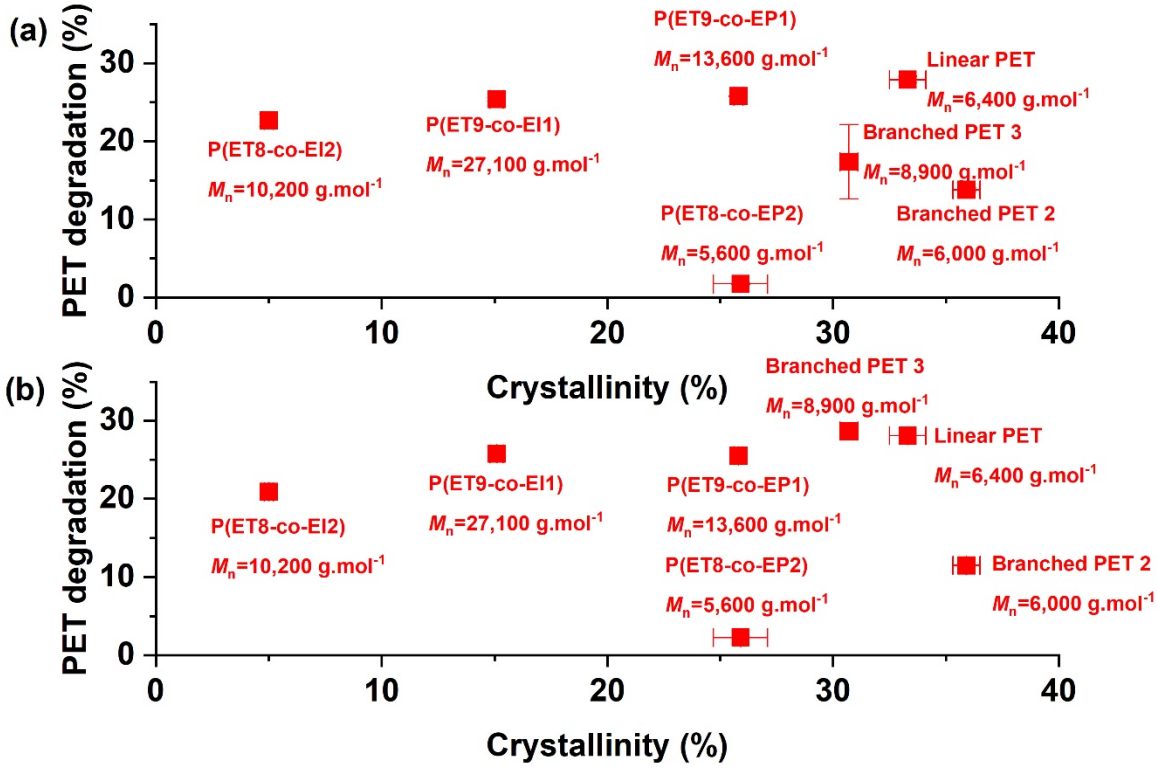

Figure 4. Percentage of degraded PET measured by HPLC of supernatant of degradation medium versus polymer crystallinity measured by DSC after (a) 24 h and (b) 72 h of incubation at 30 °C temperature. The molecular weight of each polymer before degradation is indicated.

PETase can degrade PET with modified structure. Except for branched PET 3, the percentage of degradation after 24 h and 72 h are not significantly different. This means that in these conditions, the maximum amount of degradation is plateauing after 24 h. We observed slightly higher degradation at t=24h than at t=72h for P(ET8-co-EP2) and branched PET 2, which were physically impossible. We speculate that it was due to systematic errors during the integration process (such as noise, baseline, or integration limits) or during the experimental procedure (such as variations in polymer weight or buffer volume). The broad substrate specificity of PETase is not surprising as it is a polyesterase with an open active site cleft which allows accommodation of bulky ester linkages. P(ET-co-EI)s, P(ET-co-EP)s and branched PETs are also aromatic polyesters with bulky esters linkages. The interesting

observation is that lower crystallinity does not lead to higher degradation as previously observed[17, 20, 21, 39, 42]. This suggests that the chemical structure of the substrate influences its enzymatic degradation, and its effect is stronger than the effect of crystallinity. This observation is not surprising as the modified polymers are not pure PET. Both morphology and interaction between enzyme and substrate were studied. The surface morphologies of linear PET, P(ET9-co-EI1), P(ET9-co-EP1) and branched PET 3 were observed by SEM (Figure S35 in supplementary materials). There is no significant difference of morphology, hence the degradation results shown in Table 4 and Figure 4 cannot be explained using morphological differences.

In 2017, Han et al. gave a deep insight into the mechanism of PET catalytic degradation[70]. The catalytic site of PETase involves several amino acids. NH groups of methionine and tyrosine forms H-bond with the oxygen of carbonyl group of PET adjacent to an aromatic ring. This activates the carbonyl group and facilitate the nucleophilic attack by the hydroxyl group of a serine. The hydroxyl group of the serin forms H-bond with aromatic nitrogen of a histidine and the other aromatic N of the histidine form H-bond with the carboxylic acid group of the aspartate. Even though kinking and branching do not prevent PET chains to enter in the active site of PETases, the kinking and branching are expected to affect the interactions between amino acids of the PETase and PET.

Consequently, enzymatic degradation may be slower near an ortho or a meta aromatic ring. When 20 % of EP units are inserted, the catalytic activity is most inhibited. Based on the microstructure, we would expect less inhibition of degradation with EP insertion as P(ET-co-EP)s have higher ET average sequence length. The strong inhibition of enzymatic degradation may be due to the limited reduction of crystallinity in the case of EP insertion. For EI insertion, the strong reduction in the crystallinity may partially compensate the effect of microstructure modification. It may also be due to some polymer entanglements created by a critical number of ortho rings that could prevent some polymer chains to enter in the active site of PETase. A third hypothesis is less activation of carbonyl bond by the PETase in the case of P(ET-co-EP) (more explanations are given in section 3.4. and on Figure 5)

We observe that branching reduces the enzymatic activity too. It may be due to steric hindrance in the catalytic site of PETase and the absence of reduction of crystallinity and microstructure modification that is favourable for degradation. Moreover, branched and crosslinked PET are expected to exhibit bigger volume than linear PET or PET-based copolymers which may affect the entrance of polymer chains in the active site of the PETase. However, this does not explain that after 72 h, important enzymatic degradation of branched PET 3 is observed. This remains an open issue. Finally, we do not clearly observe any significant effect of the molar mass on the enzymatic degradation within this range. Again, the effect of substrate's microstructure seems to be stronger. However, we believe it exists within higher range of M_n as commercial PETs degrade slower than the PETs we made here, whose size is smaller[19]. Such an effect was already observed previously[71].

Interactions between PETase and polymer chains

To provide further insights on the interactions of the kinks and branches, docking studies were carried out for P(ET-co-EI), P(ET-co-EP) and branched PET, with PET as the reference. PETase adopts the canonical α/β-hydrolase fold with a conserved catalytic triad S131-H208-D177 on the protein surface. In-silico docking was used to dock the PET analogues into the catalytic pocket in PETase. Our docking predicted that both, PET and modified PET, can be easily docked into the active site cleft on the surface of the PETase. One unit each of PET from the linear and modified PET is bound in a groove consisting of residues S131, H208, W156, I179, W130, Y58 and M132 from PETase. The ethylene glycol linker is located at the catalytic centre that allows the PETase to carry out hydrolysis. The side chain of S131 points towards the carbonyl carbon of PET, positioning it for nucleophilic attack. The side chain of H208 forms a hydrogen bond with the ester oxygen atom from PET and from modified PET in all the four cases. The ester oxygen atom is further involved in hydrogen bond interactions with the backbone nitrogen of residues M132 and Y58 from PETase in the case of Liner-PET, P(ET-co-EI) and branched-PET; however such an interaction was not observed in the case of P(ET-co-EP). With all four ligands, two phenyl groups located on either side of ethylene glycol liker were bound with a kink and involved

in T-stacking interactions with the side chains of W130 (except in the case of Branched-PET) and W156. In addition, the ethylene glycol linker that connects the 2nd and 3rd phenyl groups is involved in additional interactions with the residues from the extended binding pocket/groove (Figure 6). These differences in how PETase interacts with the various polymer chains provides good insight into the observed differences in the degradation behaviour of the polymers.

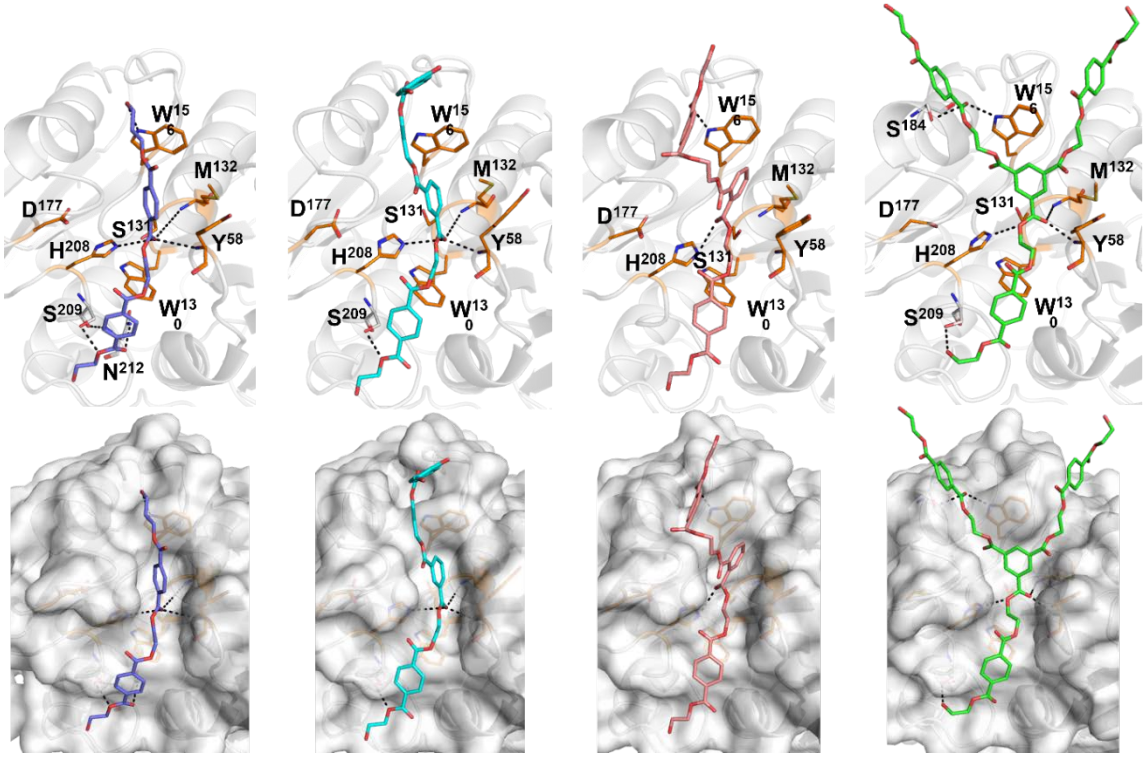

Figure 5: Structural model of PETase – PET complexes. (top) The PETase structure is shown as cartoon (grey), the catalytic triad (S131, D177 and H208) and the residues involved in binding are shown as lines (Orange carbon) and the bound ligands are shown as sticks (blue: linear PET; Cyan: P(ET-co-EI); Salmon: P(ET-co-EP); green: Branched PET). Hydrogen bond interactions are highlighted in dashed lines (black). (Bottom): Same as top, with the PETase shown as surface (grey). More details are in supporting information (Figure S36).

Conclusions

This work investigated the effects of PET and PET copolymers on PETase activity. Linear PET, P(ET-co-EI)s and P(ET-co-EP)s with different compositions, as well as branched PET with different *DB,* were synthesized from aryl chloride molecules at room temperature. Structural characterization showed that the fraction of EP units in the copolymers corresponded to the fraction of IPCl in the batch, while the synthesis of P(ET-co-EP) led to lower EP incorporation and shorter chains, likely due to side reactions. P(ET-co-EI) copolymers were found to be more random than P(ET-co-EP) copolymers. The *DB* of branched PET was lower than the fraction of TMCl present in the batch, possibly due to the accuracy of NMR measurement as branching leads to non-soluble fractions in deuterated solvent. This reduction of solubility suggests the formation of crosslinked structures. As expected, the insertion of EP and EI units in PET chains reduced the crystallinity, with a slower reduction observed for EP units due to the longer ET average sequence length. No significant reduction in crystallinity with branching was observed as *DB*s did not exceed 3%. The influence of kinking and branching on T_g was unclear from our data, as the effects of hydrogen bond formation, leading to higher T_g, and chain length likely competed with the effects of kinking and branching. Linear PET, P(ET9-co-EI1), P(ET8-co-EI2), P(ET9-co-EP1), P(ET8-co-EP2), branched PET 2 and branched PET 3 were degraded with PETase from *Ideonella sakaiensis*. This enzyme showed activity for PET with modified structure but kinking and branching inhibited its activity. Docking analysis showed that both kinking and branching affected the interactions between PETase and PET substrate, suggesting that chemical structure modifications have a stronger effect on enzyme activity than substrate crystallinity.

Supporting information

Details on syntheses and analyses can be found in Supporting information.

Acknowledgements

We acknowledge the support from National Research Foundation (NRF) under its Competitive Research Programme (Award# NRF-CRP22-2019-0005). Dr Rupali Reddy Pasula (NTU, CCEB), A/Prof Christopher Michael Fellows (University of New England), Prof Alex van Herk (Eindhoven University of Technology) and Dr Anbanandam Parthiban (ASTAR, IC2E) are acknowledged for their feedback and regular advice. We thank Dr Sung Ju Cho (NTU, MSE) for his help in the organic chemistry lab, Dr Ye Hong (NTU, SBS) for her help with NMR spectroscopy analysis, and Dr Jing Ni Chan for her help with HPLC analysis. Ying Lee Ling (NTU, MSE) is acknowledged for his help with the synthesis of branched PET.

References

(1) Nikiema, J.; Asiedu, Z. A review of the cost and effectiveness of solutions to address plastic pollution. *Environmental Science and Pollution Research* **2022**, *29* (17), 24547-24573. DOI: 10.1007/s11356-021-18038-5.

(2) Didane, N.; Giraud, S.; Devaux, E.; Lemort, G.; Capon, G. Thermal and fire resistance of fibrous materials made by PET containing flame retardant agents. *Polymer Degradation and Stability* **2012**, *97* (12), 2545-2551. DOI: 10.1016/j.polymdegradstab.2012.07.006.

(3) Jeon, H. Y.; Cho, S. H.; Mok, M. S.; Park, Y. M.; Jang, J. W. Assessment of chemical resistance of textile geogrids manufactured with PET high-performance yam. *Polymer Testing* **2005**, *24* (3), 339-345. DOI: 10.1016/j.polymertesting.2004.10.006.

(4) Azhdarpour, A. M.; Nikoudel, M. R.; Taheri, M. The effect of using polyethylene terephthalate particles on physical and strength-related properties of concrete; a laboratory evaluation. *Construction and Building Materials* **2016**, *109*, 55-62. DOI: 10.1016/j.conbuildmat.2016.01.056.

(5) Itim, B.; Philip, M. Effect of multiple extrusions and influence of PP contamination on the thermal characteristics of bottle grade recycled PET. *Polymer Degradation and Stability* **2015**, *117*, 84-89. DOI: 10.1016/j.polymdegradstab.2015.04.004.

(6) Rahimi, A.; Garcia, J. M. Chemical recycling of waste plastics for new materials production. *Nature Reviews Chemistry* **2017**, *1* (6). DOI: 10.1038/s41570-017-0046.

(7) Sinha, V.; Patel, M. R.; Patel, J. V. Pet Waste Management by Chemical Recycling: A Review. *Journal of Polymers and the Environment* **2010**, *18* (1), 8-25. DOI: 10.1007/s10924-008-0106-7.

(8) Park, S. H.; Kim, S. H. Poly (ethylene terephthalate) recycling for high value added textiles. *Fashion and Textiles* **2014**, *1* (1). DOI: 10.1186/s40691-014-0001-x.

(9) Welle, F. Twenty years of PET bottle to bottle recycling-An overview. *Resources Conservation and Recycling* **2011**, *55* (11), 865-875. DOI: 10.1016/j.resconrec.2011.04.009.

(10) Sang, T.; Wallis, C. J.; Hill, G.; Britovsek, G. J. P. Polyethylene terephthalate degradation under natural and accelerated weathering conditions. *European Polymer Journal* **2020**, *136*. DOI: 10.1016/j.eurpolymj.2020.109873.

(11) Nikles, D. E.; Farahat, M. S. New motivation for the depolymerization products derived from poly(ethylene terephthalate) (PET) waste: A review. *Macromolecular Materials and Engineering* **2005**, *290* (1), 13-30. DOI: 10.1002/mame.200400186.

(12) Tournier, V.; Duquesne, S.; Guillamot, F.; Cramail, H.; Andre, I.; Taton, D.; Marty, A. Enzymes? Power for Plastics Degradation. *Chemical Reviews* **2023**, *123* (9), 5612-5701. DOI: 10.1021/acs.chemrev.2c00644.

(13) Flores, I.; Etxeberria, A.; Irusta, L.; Calafel, I.; Vega, J. F.; Martinez-Salazar, J.; Sardon, H.; Muller, A. J. PET-ran-PLA Partially Degradable Random Copolymers Prepared by Organocatalysis: Effect of Poly(L-lactic acid) Incorporation on Crystallization and Morphology. *Acs Sustainable Chemistry & Engineering* **2019**, *7* (9), 8647-8659. DOI: 10.1021/acssuschemeng.9b00443.

(14) Muller, R. J.; Schrader, H.; Profe, J.; Dresler, K.; Deckwer, W. D. Enzymatic degradation of poly(ethylene terephthalate): Rapid hydrolyse using a hydrolase from T-fusca. *Macromolecular Rapid Communications* **2005**, *26* (17), 1400-1405. DOI: 10.1002/marc.200500410.

(15) Yoshida, S.; Hiraga, K.; Takehana, T.; Taniguchi, I.; Yamaji, H.; Maeda, Y.; Toyohara, K.; Miyamoto, K.; Kimura, Y.; Oda, K. A bacterium that degrades and assimilates poly(ethylene terephthalate). *Science* **2016**, *351* (6278), 1196-1199. DOI: 10.1126/science.aad6359.

(16) Wei, R.; von Haugwitz, G.; Pfaff, L.; Mican, J.; Badenhorst, C. P. S.; Liu, W. D.; Weber, G.; Austin, H. P.; Bednar, D.; Damborsky, J.; et al. Mechanism-Based Design of Efficient PET Hydrolases. *Acs Catalysis* **2022**, *12* (6), 3382-3396. DOI: 10.1021/acscatal.1c05856.

(17) Austin, H. P.; Allen, M. D.; Donohoe, B. S.; Rorrer, N. A.; Kearns, F. L.; Silveira, R. L.; Pollard, B. C.; Dominick, G.; Duman, R.; El Omari, K.; et al. Characterization and engineering of a plastic-degrading aromatic polyesterase. *Proceedings of the National Academy of Sciences of the United States of America* **2018**, *115* (19), E4350-E4357. DOI: 10.1073/pnas.1718804115.

(18) Ronkvist, A. M.; Xie, W. C.; Lu, W. H.; Gross, R. A. Cutinase-Catalyzed Hydrolysis of Poly(ethylene terephthalate). *Macromolecules* **2009**, *42* (14), 5128-5138. DOI: 10.1021/ma9005318.
(19) Tournier, V.; Topham, C. M.; Gilles, A.; David, B.; Folgoas, C.; Moya-Leclair, E.; Kamionka, E.; Desrousseaux, M. L.; Texier, H.; Gavalda, S.; et al. An engineered PET depolymerase to break down and recycle plastic bottles. *Nature* **2020**, *580* (7802), 216-+. DOI: 10.1038/s41586-020-2149-4.
(20) Thomsen, T. B.; Hunt, C. J.; Meyer, A. S. Influence of substrate crystallinity and glass transition temperature on enzymatic degradation of polyethylene terephthalate (PET). *New Biotechnology* **2022**, *69*, 28-35. DOI: 10.1016/j.nbt.2022.02.006.
(21) Erickson, E.; Shakespeare, T. J.; Bratti, F.; Buss, B. L.; Graham, R.; Hawkins, M. A.; Konig, G.; Michener, W. E.; Miscall, J.; Ramirez, K. J.; et al. Comparative Performance of PETase as a Function of Reaction Conditions, Substrate Properties, and Product Accumulation. *Chemsuschem* **2022**, *15* (1). DOI: 10.1002/cssc.202101932.
(22) Bersot, J. C.; Jacquel, N.; Saint-Loup, R.; Fuertes, P.; Rousseau, A.; Pascault, J. P.; Spitz, R.; Fenouillot, F.; Monteil, V. Efficiency Increase of Poly(ethylene terephthalate-co-isosorbide terephthalate) Synthesis using Bimetallic Catalytic Systems. *Macromolecular Chemistry and Physics* **2011**, *212* (19), 2114-2120. DOI: 10.1002/macp.201100146.
(23) Giol, E. D.; Van den Brande, N.; Van Mele, B.; Van Vlierberghe, S.; Dubruel, P. Single-step solution polymerization of poly(alkylene terephthalate)s: synthesis parameters and polymer characterization. *Polymer International* **2018**, *67* (3), 292-300. DOI: 10.1002/pi.5508.
(24) Manaresi, P.; Munari, A.; Pilati, F.; Alfonso, G. C.; Russo, S.; Sartirana, M. L. Synthesis and characterization of highly-branched poly(ethylene-terephthalate). *Polymer* **1986**, *27* (6), 955-960. DOI: 10.1016/0032-3861(86)90311-3.
(25) de Ilarduya, A. M.; Kint, D. P. R.; Munoz-Guerra, S. Sequence analysis of poly(ethylene terephthalate-co-isophthalate) copolymers by C-13 NMR. *Macromolecules* **2000**, *33* (12), 4596-4598.
(26) Karayiannis, N. C.; Mavrantzas, V. G.; Theodorou, D. N. Detailed atomistic simulation of the segmental dynamics and barrier properties of amorphous poly(ethylene terephthalate) and poly(ethylene isophthalate). *Macromolecules* **2004**, *37* (8), 2978-2995. DOI: 10.1021/ma0352577.
(27) Kruse, M.; Wagner, M. H. Rheological and molecular characterization of long-chain branched poly(ethylene terephthalate). *Rheologica Acta* **2017**, *56* (11), 887-904. DOI: 10.1007/s00397-017-1043-y.
(28) Light, R. R.; Seymour, R. W. Effect of sub-Tg relaxations on the gas-transport properties of polyesters. *Polymer Engineering and Science* **1982**, *22* (14), 857-864. DOI: 10.1002/pen.760221402.
(29) Lee, S. W.; Ree, M.; Park, C. E.; Jung, Y. K.; Park, C. S.; Jin, Y. S.; Bae, D. C. Synthesis and non-isothermal crystallization behaviors of poly(ethylene isophthalate-co-terephthalate)s. *Polymer* **1999**, *40* (25), 7137-7146. DOI: 10.1016/s0032-3861(99)00119-6.
(30) Arayesh, H.; Ebrahimi, N. G.; Khaledi, B.; Esfahani, M. K. Introducing four different branch structures in PET by reactive processing--A rheological investigation. *Journal of Applied Polymer Science* **2020**, *137* (41). DOI: 10.1002/app.49243.
(31) Dhavalikar, R.; Yamaguchi, M.; Xanthos, A. Molecular and structural analysis of a triepoxide-modified poly(ethylene terephthalate) from rheological data. *Journal of Polymer Science Part a-Polymer Chemistry* **2003**, *41* (7), 958-969. DOI: 10.1002/pola.10641.
(32) Jayakannan, M.; Ramakrishnan, S. Effect of branching on the crystallization kinetics of poly(ethylene terephthalate). *Journal of Applied Polymer Science* **1999**, *74* (1), 59-66. DOI: 10.1002/(sici)1097-4628(19991003)74:1<59::Aid-app6>3.0.Co;2-0.
(33) Chen, M. H.; Lai, C. C.; Chen, H. L.; Lin, C. H.; Hsiao, H. T.; Liu, L. C.; Chen, C. M. Preparation of long-chain branched polyethylene terephthalates (PETs), and crystallization behaviors, thermal characteristics, and hydrolysis resistance of their biaxially stretching films. *Journal of Physics and Chemistry of Solids* **2019**, *129*, 354-367. DOI: 10.1016/j.jpcs.2019.01.031.
(34) Ubach, J.; de Ilarduya, A. M.; Quintana, R.; Alla, A.; Rude, E.; Munoz-Guerra, S. Poly(ethylene terephthalate-co-isophthalate) Copolyesters Obtained from Ethylene Terephthalate and Isophthalate Oligomers. *Journal of Applied Polymer Science* **2010**, *115* (3), 1823-1830. DOI: 10.1002/app.31308.

(35) Li, B.; Yu, J.; Lee, S.; Ree, M. Poly(ethylene terephthalate co ethylene isophthalate) - relationship between physical properties and chemical structures. *European Polymer Journal* **1999**, *35* (9), 1607-1610. DOI: 10.1016/s0014-3057(98)00252-3.
(36) Yu, J. Y.; Li, B. Z.; Lee, S. W.; Ree, M. H. Relationship between physical properties and chemical structures of poly(ethylene terephthalate-co-ethylene isophthalate). *Journal of Applied Polymer Science* **1999**, *73* (7), 1191-1195. DOI: 10.1002/(sici)1097-4628(19990815)73:7<1191::Aid-app12>3.0.Co;2-s.
(37) Avarzman, A. M.; Rafizadeh, M.; Taromi, F. A. Branched polyester based on the polyethylene tere/iso phthalate and trimellitic anhydride as branching agent. *Polymer Bulletin* **2022**, *79* (8), 6099-6121. DOI: 10.1007/s00289-021-03802-x.
(38) Cui, Y. L.; Chen, Y. C.; Liu, X. Y.; Dong, S. J.; Tian, Y. E.; Qiao, Y. X.; Mitra, R.; Han, J.; Li, C. L.; Han, X.; et al. Computational Redesign of a PETase for Plastic Biodegradation under Ambient Condition by the GRAPE Strategy. *Acs Catalysis* **2021**, *11* (3), 1340-1350. DOI: 10.1021/acscatal.0c05126.
(39) Wei, R.; Breite, D.; Song, C.; Grasing, D.; Ploss, T.; Hille, P.; Schwerdtfeger, R.; Matysik, J.; Schulze, A.; Zimmermann, W. Biocatalytic Degradation Efficiency of Postconsumer Polyethylene Terephthalate Packaging Determined by Their Polymer Microstructures. *Advanced Science* **2019**, *6* (14). DOI: 10.1002/advs.201900491.
(40) Menzel, T.; Weigert, S.; Gagsteiger, A.; Eich, Y.; Sittl, S.; Papastavrou, G.; Ruckdaschel, H.; Altstadt, V.; Hocker, B. Impact of Enzymatic Degradation on the Material Properties of Poly(Ethylene Terephthalate). *Polymers* **2021**, *13* (22). DOI: 10.3390/polym13223885.
(41) Tarazona, N. A.; Wei, R.; Brott, S.; Pfaff, L.; Bornscheuer, U. T.; Lendlein, A.; Machatschek, R. Rapid depolymerization of poly(ethylene terephthalate) thin films by a dual-enzyme system and its impact on material properties. *Chem Catalysis* **2022**, *2* (12), 3573-3589. DOI: 10.1016/j.checat.2022.11.004.
(42) Thomsen, T. B.; Schubert, S.; Hunt, C. J.; Borch, K.; Jensen, K.; Brask, J.; Westh, P.; Meyer, A. S. Rate Response of Poly(Ethylene Terephthalate)-Hydrolases to Substrate Crystallinity: Basis for Understanding the Lag Phase. *Chemsuschem* **2023**. DOI: 10.1002/cssc.202300291.
(43) Pasula, R. R.; Lim, S.; Ghadessy, F. J.; Sana, B. The influences of substrates' physical properties on enzymatic PET hydrolysis: Implications for PET hydrolase engineering. *Engineering Biology* **2022**, *6* (1), 17-22. DOI: https://doi.org/10.1049/enb2.12018.
(44) Son, H. F.; Cho, I. J.; Joo, S.; Seo, H.; Sagong, H. Y.; Choi, S. Y.; Lee, S. Y.; Kim, K. J. Rational Protein Engineering of Thermo-Stable PETase from Ideonella sakaiensis for Highly Efficient PET Degradation. *Acs Catalysis* **2019**, *9* (4), 3519-3526. DOI: 10.1021/acscatal.9b00568.
(45) T.D.W., C. igh-resolution NMR techniques in organic chemistry. *2nd ed., Elsevier, Science, Amsterdam,* **2009**.
(46) Mehta, A.; Gaur, U.; Wunderlich, B. Equilibrium melting parameters of poly(ethylene terephthalate). *Journal of Polymer Science: Polymer Physics Edition* **1978**, *16* (2), 289-296. DOI: https://doi.org/10.1002/pol.1978.180160209.
(47) Vertommen, M. A. M. E.; Nierstrasz, V. A.; Veer, M. v. d.; Warmoeskerken, M. M. C. G. Enzymatic surface modification of poly(ethylene terephthalate). *Journal of Biotechnology* **2005**, *120* (4), 376-386. DOI: https://doi.org/10.1016/j.jbiotec.2005.06.015.
(48) Kaminski, G. A.; Friesner, R. A.; Tirado-Rives, J.; Jorgensen, W. L. Evaluation and reparametrization of the OPLS-AA force field for proteins via comparison with accurate quantum chemical calculations on peptides. *Journal of Physical Chemistry B* **2001**, *105* (28), 6474-6487. DOI: 10.1021/jp003919d.
(49) Schrodinger, version 9.0. *Schrödinger* **2009**, *LLC, New York, NY, 2009*.
(50) Friesner, R. A.; Banks, J. L.; Murphy, R. B.; Halgren, T. A.; Klicic, J. J.; Mainz, D. T.; Repasky, M. P.; Knoll, E. H.; Shelley, M.; Perry, J. K.; et al. Glide: A new approach for rapid, accurate docking and scoring. 1. Method and assessment of docking accuracy. *Journal of Medicinal Chemistry* **2004**, *47* (7), 1739-1749. DOI: 10.1021/jm0306430.
(51) Kannan, S.; Pradhan, M. R.; Cherian, J.; Joseph, T. L.; Poh, Z. Y.; An, Y. H.; Melvyn, H.; Liu, B. P.; Jeffrey, H.; Nacro, K.; et al. Small Molecules Targeting the Inactive Form of the Mnk1/2 Kinases. *Acs Omega* **2017**, *2* (11), 7881-7891. DOI: 10.1021/acsomega.7b01403.

(52) Case, D. e. a. Amber 18. . *University of California, San Francisco.*
(53) Maier, J. A.; Martinez, C.; Kasavajhala, K.; Wickstrom, L.; Hauser, K. E.; Simmerling, C. ff14SB: Improving the Accuracy of Protein Side Chain and Backbone Parameters from ff99SB. *Journal of Chemical Theory and Computation* **2015**, *11* (8), 3696-3713. DOI: 10.1021/acs.jctc.5b00255.
(54) Wang, J. M.; Wolf, R. M.; Caldwell, J. W.; Kollman, P. A.; Case, D. A. Development and testing of a general amber force field. *Journal of Computational Chemistry* **2004**, *25* (9), 1157-1174. DOI: 10.1002/jcc.20035.
(55) Jorgensen, W. L.; Chandrasekhar, J.; Madura, J. D.; Impey, R. W.; Klein, M. L. Comparison of simple potential functions for simulating liquid water. *Journal of Chemical Physics* **1983**, *79* (2), 926-935. DOI: 10.1063/1.445869.
(56) Darden, T.; York, D.; Pedersen, L. Particle mesh ewald - AN N.LOG(N) method for ewald sums in large systems. *Journal of Chemical Physics* **1993**, *98* (12), 10089-10092. DOI: 10.1063/1.464397.
(57) Miyamoto, S.; Kollman, P. A. Settle - An analytical version of the SHAKE and RATTLE algorithm for rigid water models. *Journal of Computational Chemistry* **1992**, *13* (8), 952-962. DOI: 10.1002/jcc.540130805.
(58) Humphrey, W.; Dalke, A.; Schulten, K. VMD: Visual molecular dynamics. *Journal of Molecular Graphics & Modelling* **1996**, *14* (1), 33-38. DOI: 10.1016/0263-7855(96)00018-5.
(59) De Lano, W. The PyMOL molecular graphics system. *San Carlos CA, USA: De Lano Scientific* **2002**.
(60) Maniego, A. R.; Sutton, A. T.; Gaborieau, M.; Castignolles, P. Assessment of the Branching Quantification in Poly(acrylic acid): Is It as Easy as It Seems? *Macromolecules* **2017**, *50* (22), 9032-9041. DOI: 10.1021/acs.macromol.7b01411.
(61) Lena, J. B.; Goroncy, A. K.; Thevarajah, J. J.; Maniego, A. R.; Russell, G. T.; Castignolles, P.; Gaborieau, M. Effect of transfer agent, temperature and initial monomer concentration on branching in poly(acrylic acid): A study by C-13 NMR spectroscopy and capillary electrophoresis. *Polymer* **2017**, *114*, 209-220. DOI: 10.1016/j.polymer.2017.01.030.
(62) Schmitz, S.; Dona, A. C.; Castignolles, P.; Gilbert, R. G.; Gaborieau, M. Assessment of the Extent of Starch Dissolution in Dimethyl Sulfoxide by H-1 NMR Spectroscopy. *Macromolecular Bioscience* **2009**, *9* (5), 506-514. DOI: 10.1002/mabi.200800244.
(63) Jayakannan, M.; Ramakrishnan, S. Synthesis and thermal analysis of branched and "kinked" poly(ethylene terephthalate). *Journal of Polymer Science Part a-Polymer Chemistry* **1998**, *36* (2), 309-317. DOI: 10.1002/(sici)1099-0518(19980130)36:2<309::Aid-pola14>3.3.Co;2-q.
(64) McKee, M. G.; Unal, S.; Wilkes, G. L.; Long, T. E. Branched polyesters: recent advances in synthesis and performance. *Progress in Polymer Science* **2005**, *30* (5), 507-539. DOI: 10.1016/j.progpolymsci.2005.01.009.
(65) Zhu, Q.; Wu, J. L.; Tu, C. L.; Shi, Y. F.; He, L.; Wang, R. B.; Zhu, X. Y.; Yan, D. Y. Role of Branching Architecture on the Glass Transition of Hyperbranched Polyethers. *Journal of Physical Chemistry B* **2009**, *113* (17), 5777-5780. DOI: 10.1021/jp900992e.
(66) Foix, D.; Khalyavina, A.; Morell, M.; Voit, B.; Lederer, A.; Ramis, X.; Serra, A. The Effect of the Degree of Branching in Hyperbranched Polyesters Used as Reactive Modifiers in Epoxy Thermosets. *Macromolecular Materials and Engineering* **2012**, *297* (1), 85-94. DOI: 10.1002/mame.201100078.
(67) Wooley, K. L.; Frechet, J. M. J.; Hawker, C. J. Influence of Shape on the Reactivity and Properties of Dendritic, Hyperbranched and Llinear Aromatic Polyesters. *Polymer* **1994**, *35* (21), 4489-4495. DOI: 10.1016/0032-3861(94)90793-5.
(68) Khalyavina, A.; Haussler, L.; Lederer, A. Effect of the degree of branching on the glass transition temperature of polyesters. *Polymer* **2012**, *53* (5), 1049-1053. DOI: 10.1016/j.polymer.2012.01.020.
(69) Mo, Z.; Zhang, H. The Degree of Crystallinity in Polymers by Wide-Angle X-Ray Diffraction (Waxd). *Journal of Macromolecular Science, Part C* **1995**, *35* (4), 555-580. DOI: 10.1080/15321799508021751.
(70) Han, X.; Liu, W. D.; Huang, J. W.; Ma, J. T.; Zheng, Y. Y.; Ko, T. P.; Xu, L. M.; Cheng, Y. S.; Chen, C. C.; Guo, R. T. Structural insight into catalytic mechanism of PET hydrolase. *Nature Communications* **2017**, *8*. DOI: 10.1038/s41467-017-02255-z.

(71) Pfaff, L.; Gao, J.; Li, Z. S.; Jaeckering, A.; Weber, G.; Mican, J.; Chen, Y. P.; Dong, W. L.; Han, X.; Feiler, C. G.; et al. Multiple Substrate Binding Mode-Guided Engineering of a Thermophilic PET Hydrolase. *Acs Catalysis* **2022**. DOI: 10.1021/acscatal.2c02275.

TABLE OF CONTENT

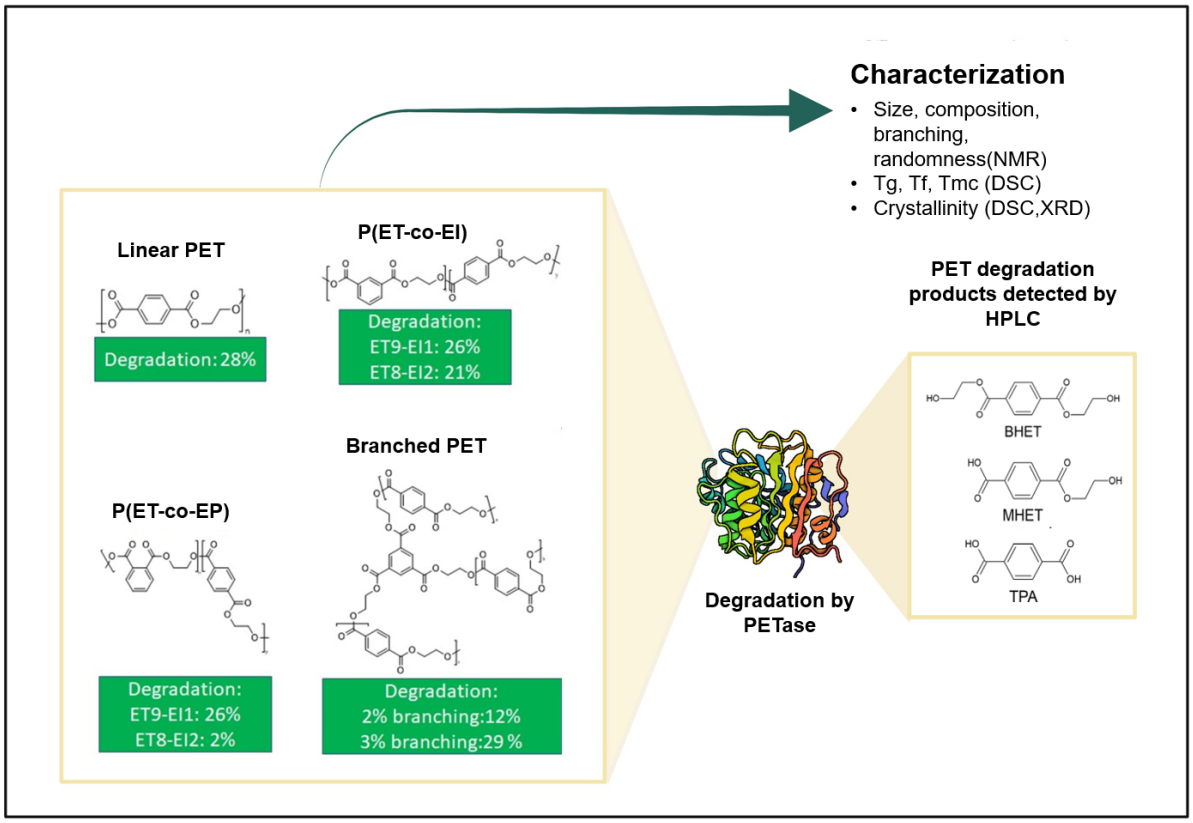

Synopsis: Enzymatic degradation of PET-based polymers allows recovering monomers for further use with a green process and reducing pollution.